

**LA-6893-PR**

Progress Report

Special Distribution

Issued: July 1977

C.3

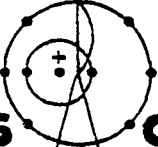
**CIC-14 REPORT COLLECTION  
REPRODUCTION  
COPY**

**Applied Nuclear Data  
Research and Development  
January 1—March 31, 1977**

Compiled by

C. I. Baxman  
P. G. Young



  
**los alamos**  
**scientific laboratory**  
of the University of California  
LOS ALAMOS, NEW MEXICO 87545

 An Affirmative Action/Equal Opportunity Employer

The four most recent reports in this series, unclassified, are LA-6472-PR, LA-6560-PR, LA-6723-PR, and LA-6754-PR.

This work was performed under the auspices of the Nuclear Regulatory Commission, the Electric Power Research Institute, the Air Force Weapons Laboratory, and the US Energy Research and Development Administration's Divisions of Military Application, Reactor Development and Demonstration, Physical Research, and Magnetic Fusion Energy.

This report was prepared as an account of work sponsored by the United States Government. Neither the United States nor the United States Energy Research and Development Administration, nor any of their employees, nor any of their contractors, subcontractors, or their employees, makes any warranty, express or implied, or assumes any legal liability or responsibility for the accuracy, completeness, or usefulness of any information, apparatus, product, or process disclosed, or represents that its use would not infringe privately owned rights.

## CONTENTS

I. THEORY AND EVALUATION OF NUCLEAR CROSS SECTIONS.....	1
A. R-Matrix Analysis of the ${}^7\text{Li}$ System.....	1
B. Evaluation of ${}^{10}\text{B}$ Cross Sections.....	2
C. Resonance Parameters from the R-Matrix.....	2
D. Calculation of ${}^{88}\text{Y}$ and ${}^{87}\text{Y}$ Capture Cross Sections Between 0.01 and 0.25 MeV.....	3
E. Evaluation of the ${}^{89}\text{Y}(n,\gamma)$ Cross Section from 0.001 to 20 MeV.....	5
F. Calculation of 15-MeV Neutron-Induced Charged-Particle Spectra on Stainless Steel 316.....	5
G. Calculation of Proton-Induced Reactions up to 40 MeV...	7
H. Optical Model and Coupled-Channel Analysis.....	7
I. $n + {}^9\text{Be}$ Cross Section Evaluation.....	9
J. Reevaluation of Neutron-Induced Cross Sections for ${}^{237}\text{U}$ and ${}^{239}\text{Pu}$ .....	9
K. Electron and Photon Spectra Between 1 and 1000 s After a Fission Burst.....	10
II. NUCLEAR CROSS SECTION PROCESSING.....	11
A. The MATXS1 Cross Section Library.....	11
B. TRANSX.....	13
C. Collapse Theory.....	14
D. PCS Calculations.....	17
E. Elastic Removal Schemes.....	18
F. Elastic Removal F-Factor Effects.....	19
G. Space-Shielding Cross Sections for Pebble-Bed High-Temperature Reactors.....	20
H. Pointwise Cross Section Space Shielding in Doubly Heterogeneous Reactors.....	20
I. Cross Sections for HTGR Safety Research.....	21
III. CONSISTENCY ANALYSIS OF DIFFERENTIAL AND INTEGRAL NEUTRONICS DATA: THERMONUCLEAR TRITIUM PRODUCTION.....	21
IV. FISSION-PRODUCT, ACTINIDE, AND DECAY DATA.....	24
A. Fission Yield Theory.....	24
B. ENDF/B Phenomenological Yield Model Improvements.....	28
C. Short-Irradiation Fission-Product Beta Spectra and Total Energy Calculations Versus Experiment.....	28
D. Analytic Fitting of Summation Calculations of Delayed Energy Spectra from Fission Products.....	29
E. Decay Heat Standard ANS 5.1.....	29
REFERENCES.....	34

LOS ALAMOS NATL. LAB. LIBS.



3 9338 00402 0912

APPLIED NUCLEAR DATA RESEARCH AND DEVELOPMENT  
QUARTERLY PROGRESS REPORT  
January 1 - March 31, 1977

Compiled by

C. I. Baxman and P. G. Young

ABSTRACT

This progress report describes the activities of the Los Alamos Nuclear Data Group for the period January 1 through March 31, 1977. The topical content is summarized in the contents.

---

I. THEORY AND EVALUATION OF NUCLEAR CROSS SECTIONS

A. R-Matrix Analysis of the  ${}^7\text{Li}$  System (G. Hale and D. Dodder [T-9])

The  ${}^6\text{Li}(n,t){}^4\text{He}$  cross section is of interest in applications primarily as a standard neutron cross section at low energies, but it is also important in the determination of tritium breeding in  ${}^6\text{Li}$ -enriched fuels. Our multichannel R-matrix analysis of this system has been directed at understanding data for all the reactions open at excitation energies below 10.5 MeV in terms of resonances in  ${}^7\text{Li}$ .

We have found that the behavior of even the low-energy  ${}^6\text{Li}(n,t)$  cross section is strongly influenced by high-lying states. In particular, the  $1/v$  dependence of the integrated cross section and the pronounced asymmetry of the angular distribution at low energies appear to come from the presence of a  $3/2^+$  resonance at ~11.3 MeV excitation energy, and higher lying levels in the  $1/2^+$  state. It is possible one of the  $1/2^+$  levels may correspond to the broad structure observed at ~16.8-MeV excitation energy in  ${}^7\text{Li}$ . These results were presented in March at the International Specialists Symposium on Neutron Standards and Applications.

Recently Dodder, in collaboration with Biegert and Baker from Rice University, has started analyzing data from the  ${}^7\text{Be}$  system simultaneously with data

from  ${}^7\text{Li}$ , using charge-symmetric constraints to relate the R-matrix parameters of the mirror systems. Preliminary indications are that the neutron cross sections for  ${}^6\text{Li}$  from that analysis are quite similar to those obtained from analyzing the  ${}^7\text{Li}$  data alone. One has increased confidence, however, in the results of an analysis that accounts for data from all the 7-nucleon reactions simultaneously.

#### B. Evaluation of ${}^{10}\text{B}$ Cross Sections (G. Hale and L. Stewart)

The neutron cross sections for  ${}^{10}\text{B}$  at energies below 1 MeV, including the important  ${}^{10}\text{B}(n,\alpha)$  standard cross sections, were obtained last year from a multichannel R-matrix analysis of reactions in the  ${}^{11}\text{B}$  system.<sup>2</sup> In order to produce the Version V Evaluated Nuclear Data File (ENDF/B) for  ${}^{10}\text{B}$ , these cross sections have been matched to the existing ENDF/B-IV cross sections in the vicinity of 1 MeV. The cross sections, angular distributions, and spectra have been added for capture gamma rays (MT=102). Complete covariance information for the neutron cross sections below 1 MeV, calculated from the covariances of the R-matrix parameters, is provided in File 33. The evaluation, temporarily labeled MAT number 5010, is being sent to Brookhaven National Laboratory for distribution.

#### C. Resonance Parameters from the R-Matrix (G. M. Hale)

The parameters of the R-matrix, although fundamental from the nuclear theory point of view, have no simple correspondence with the observed widths and positions of anomalies in the experimental data. We are investigating different ways of extracting "resonance parameters" from the R-matrix in order to facilitate comparison with numbers obtained directly from measurements.

Last quarter we described a method based on the real poles and residues of the resonant Q-matrix ( $Q_R$ ), which is a multilevel extension of the prescription commonly used to define resonance parameters from a single-level R-matrix. This quarter we have implemented a similar method based on the complex poles and residues of the collision matrix. The definition of positions and widths for the resonance states then parallels that given by Humblet<sup>3</sup> for the parameters of his S-matrix expansion. These resonance parameters have the formal advantage of being independent of matching radius in the external region,<sup>3,4</sup> unlike those obtained from considering  $Q_R$ .

Starting from the same R-matrix parameters, we have noticed interesting differences in the resonance parameters obtained from the real ( $Q_R$ ) and complex (S) pole prescriptions. In the case of the  ${}^7\text{Li}$  analysis described in Sec. I.A., for instance, the parameters of the low-lying resonances were similar using the two different methods, but the width of a  $7/2^-$  resonance at  $\sim 9.6$ -MeV excitation energy in  ${}^7\text{Li}$  turned out to be about four times as wide using the real prescription as that found using the complex prescription. The width of the anomaly in the experimental data appears to be much closer to that given by considering the complex poles of the S-matrix. We are comparing the results of the two methods in other cases to see if the S-matrix prescription generally gives positions and widths closer to those observed in the experimental data.

D. Calculation of  ${}^{88}\text{Y}$  and  ${}^{87}\text{Y}$  Capture Cross Sections Between 0.01 and 0.25 MeV (E. D. Arthur)

Statistical model calculations of the  ${}^{88}\text{Y}$  and  ${}^{87}\text{Y}$  capture cross sections have been made using input parameters  $\Gamma_\gamma$  (the average gamma-ray width for S-wave resonances) and  $\langle D \rangle$  (the observed S-wave level spacing) obtained from a study of the systematic behavior of these quantities for nuclei in the mass region  $A = 85$  to  $105$ . With the parameterizations used, theoretical  $\Gamma_\gamma$  values lie generally within 25% of available experimental values, while calculated  $\langle D \rangle$  values agree generally to within 35% of the corresponding experimental value. Values obtained for  $\langle D \rangle$  and  $\Gamma_\gamma$  in the  $n + {}^{88}\text{Y}$  system were 93 and 0.17 eV; for  $n + {}^{87}\text{Y}$  they were 236 and 0.165 eV, respectively.

The solid lines in Figs. 1 and 2 show the calculated capture cross sections for  ${}^{88}\text{Y}$  and  ${}^{87}\text{Y}$  while the dotted lines indicate the errors ( $\sim 45\%$ ) estimated for the calculation. This error estimate results from adding in quadrature the errors associated with  $\Gamma_\gamma$  and  $\langle D \rangle$  described above.

In Fig. 3 experimental values (open circles) of 24-keV neutron-capture cross sections are plotted as a function of the number of neutrons for targets having odd  $Z$ . The effect of the closed neutron shell at  $N = 50$  is apparent. Also shown and indicated by closed circles are the results of the present calculations along with their estimated errors. Both calculated values seem to be in reasonable agreement with values expected from systematics in this mass region.

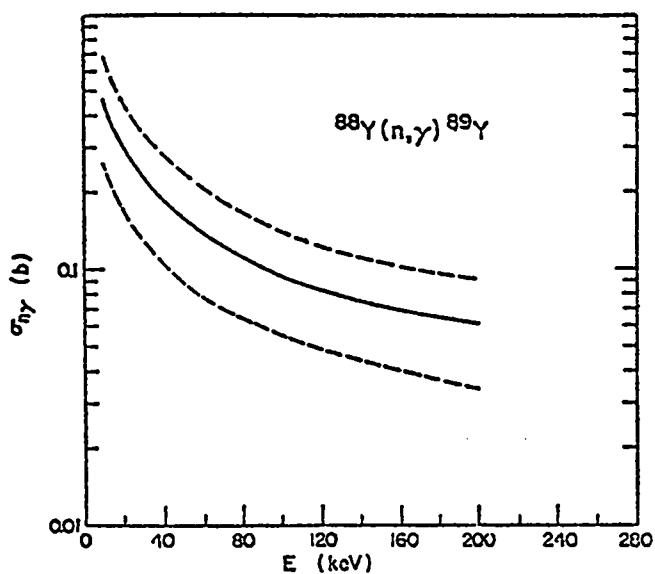


Fig. 1. Calculated (solid lines)  $^{88}\text{Y}(n,\gamma)$  cross sections with their estimated errors (dotted lines).

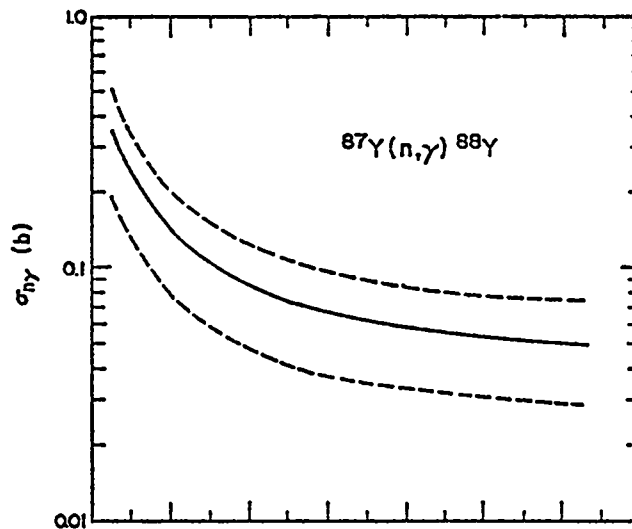


Fig. 2.  $^{87}\text{Y}(n,\gamma)$  calculated cross section and errors.

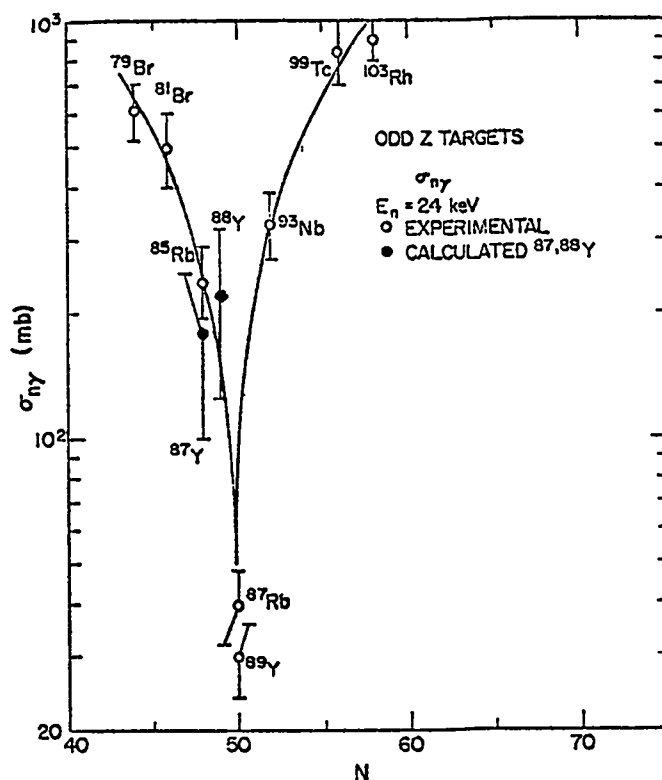


Fig. 3. Systematics of 24-keV neutron capture cross sections for odd Z targets. Open circles are experimental points; closed circles are the calculated  $^{88}\text{Y}$  and  $^{87}\text{Y}$  values.

E. Evaluation of the  $^{89}\text{Y}(n,\gamma)$  Cross Section from 0.001 to 20 MeV.  
(E. D. Arthur)

In general, existing evaluations of the  $^{89}\text{Y}(n,\gamma)$  cross section fail to include effects in the high-energy capture cross section resulting from giant dipole resonance (GDR) capture. Using a statistical model calculation along with a "preequilibrium" type treatment of the high-energy capture process to include direct-semidirect capture effects, we have calculated the  $^{89}\text{Y}$  capture cross section from 0.01 to 20 MeV. At lower energies, because of resonance structure in the capture cross sections, the data of Bergman<sup>5</sup> were used between 0.001 and 0.01 MeV. The calculated cross section is shown in Fig. 4, along with representative experimental data. Evident in the region from 10 to 15 MeV is the effect of the GDR which causes the capture cross section to rise to about 2 mb.

F. Calculation of 15-MeV Neutron-Induced Charged-Particle Spectra on Stainless Steel 316 (E. D. Arthur and P. G. Young)

We have calculated charged-particle cross sections and spectra induced by neutrons on stainless steel 316 in order to compare with the recent measurement of Haight et al.<sup>6</sup> The calculations were made using the preequilibrium-statistical model code GNASH and employed global values for preequilibrium, level density, and optical model parameters.

In order to compare with the experimental data, we calculated proton- and alpha-particle spectra and cross sections for 15 MeV neutrons on  $^{54}\text{Fe}$ ,  $^{56}\text{Fe}$ ,  $^{50}\text{Cr}$ ,  $^{52}\text{Cr}$ ,  $^{58}\text{Ni}$ , and  $^{60}\text{Ni}$  and combined the results appropriately for stainless steel 316. The calculations are compared with the experimental spectrum results in Fig. 5. (The dashed portion of the calculated proton spectra indicates regions where low-energy protons may not have been detected experimentally.) In Table I, the comparison between integrated experimental and theoretical cross sections is made. These results are typical of the general type of agreement in spectral shapes and total yields obtained from GNASH calculations near 15 MeV using global parameters.

TABLE I

COMPARISON OF ANGLE-INTEGRATED EXPERIMENTAL  
 AND CALCULATED CROSS SECTIONS FOR 15-MeV NEUTRONS ON SS-316

<u>Emitted Particle</u>	<u><math>\sigma</math> Experimental (mb)</u>	<u><math>\sigma</math> Calculated (mb)</u>
Proton	252 ± 38	316 ( $E_p > 1.5$ MeV)
Alpha	48 ± 7	45
Deuteron	8 ± 2	9

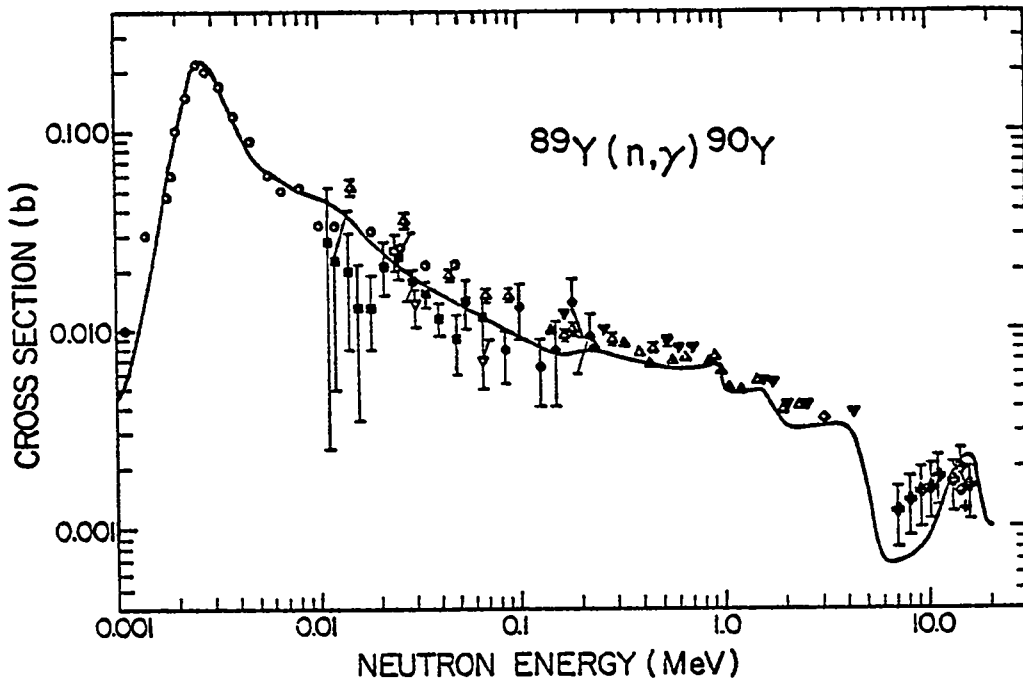


Fig. 4.

The evaluated  $^{88}\text{Y}(n,\gamma)$  cross section compared to experimental data.

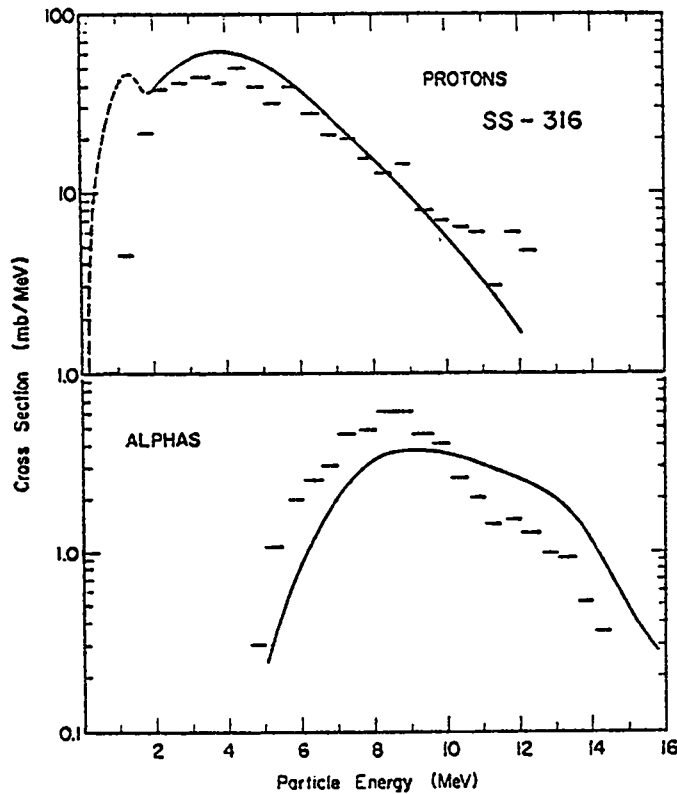


Fig. 5.

Measured and calculated proton and alpha spectra from 15-MeV neutron bombardment of stainless steel 316. The calculated results are represented by solid curves.

G. Calculation of Proton-Induced Reactions up to 40 MeV (E. D. Arthur and P. G. Young)

Intended use of 35-40 MeV deuteron beams on Li targets to produce neutrons to simulate radiation damage effects occurring in fusion reactors will probably require neutron cross-section data up to neutron energies of 40 MeV. Since little neutron-induced reaction data exists above 20 MeV, model code calculations will be an important source for the necessary cross sections. In order to test the preequilibrium-statistical model code GNASH at high energies, we have calculated reaction cross sections on  $^{89}\text{Y}$  and  $^{169}\text{Tm}$  induced by protons up to 40 MeV. The calculations used global preequilibrium and level density values and employed the following global optical model parameter sets:

$^{89}\text{Y}$ : Protons - Becchetti-Greenlees<sup>7</sup>  
Neutrons - Wilmore-Hodgson<sup>8</sup>

$^{169}\text{Tm}$ : Protons - Perey<sup>9</sup>  
Neutrons - Wilmore-Hodgson<sup>8</sup>

The calculations for  $p + ^{89}\text{Y}$  reactions are compared with experimental measurements<sup>10,11</sup> in Figs. 6 and 7. It should be noted that the energy scale of the measurements in Ref. 11 has a relatively large uncertainty, and we have shifted the measured (p,2n), (p,3n), (p,pn), and (p,p2n) cross sections downward in energy by 2 MeV. This is the energy shift needed to bring (p,n) data from Ref. 11 into agreement with the data of Ref. 10 where proton beam energies were known quite accurately. In Fig. 8, the calculations are compared with measurements of (p,n), (p,3n), and (p,4n) reactions on  $^{169}\text{Tm}$ .<sup>12</sup> Generally, the agreement between the calculations and experimental data is quite accurate considering input parameters were not adjusted in the calculation.

H. Optical Model and Coupled-Channel Analysis (D. G. Madland and P. G. Young)

Work is continuing on the development of coupled-channel transmission coefficients to be used, for example, in statistical compound nucleus codes such as GNASH<sup>13</sup> or COMNUC.<sup>14</sup> The code JUKARL<sup>15</sup> calculates a coupled-channel transmission coefficient matrix for each set of entrance-channel quantum numbers (J, $\pi$ ). The total transmission coefficient matrix is thus generated by the set [(J, $\pi$ )]. The total matrix has been calculated for  $n + ^{238}\text{U}$ ,  $n + ^{175}\text{Lu}$ , and  $n + ^{169}\text{Tm}$  examples and has, in each case, been compared to the corresponding spherical optical model transmission coefficients. The next step is apparently a mechanical

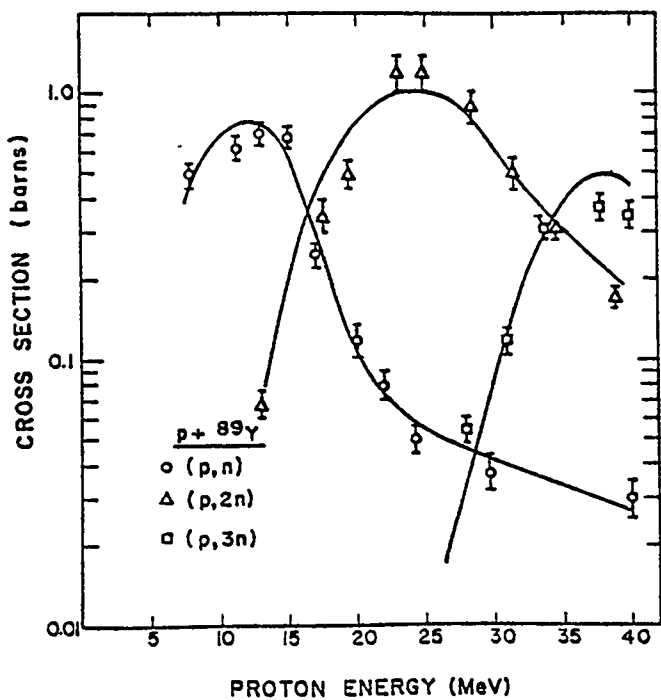


Fig. 6.  
Experimental and calculated  $^{89}\text{Y}(p,xn)$  values.

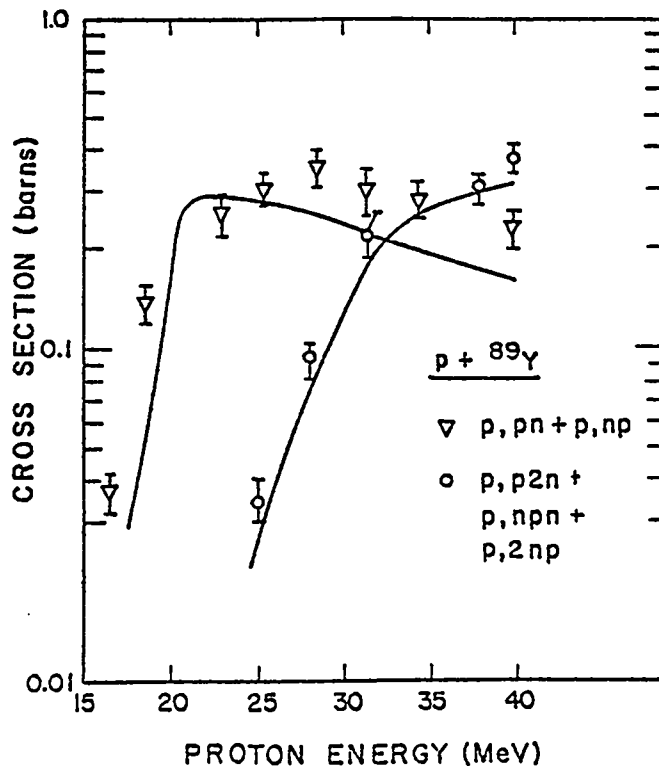


Fig. 7.  
 $^{89}\text{Y}(p,pxn)$  experimental and calculated values.

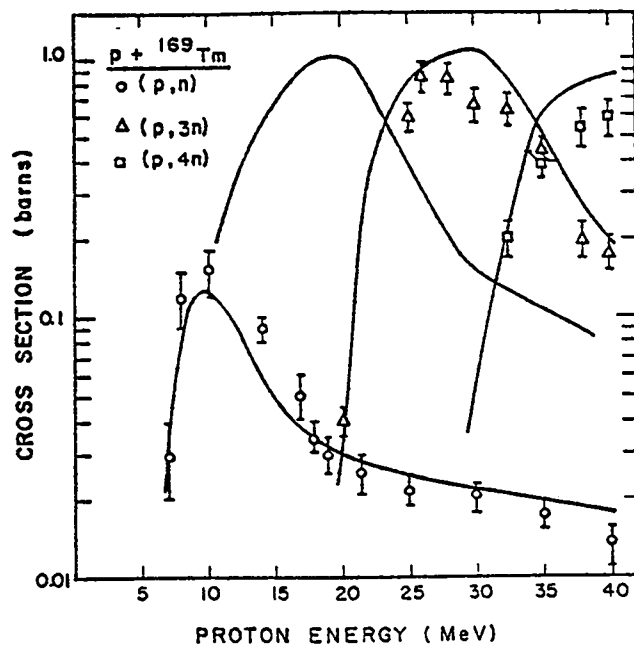


Fig. 8,  
 $^{169}\text{Tm}(p,xn)$  reactions.

one, that is, to cast the transmission coefficient matrix into a form that is readily assimilated by the statistical codes.

I.  $n + {}^9\text{Be}$  Cross-Section Evaluation (P. G. Young, L. Stewart, R. E. MacFarlane, and D. W. Muir)

An evaluation of selected neutron-induced cross sections for  ${}^9\text{Be}$  has been completed and incorporated into the ENDF/B-V evaluation from Livermore. Particular emphasis was placed on accurately representing the neutron emission spectra from (n,2n) reactions, as measured recently at Los Alamos.<sup>16</sup> In addition, the total cross section was updated above 500 keV to include new measurements from the National Bureau of Standards (NBS)<sup>17</sup> and Los Alamos.<sup>18</sup>

The ENDF/B formats are presently not suited for accurate representation of energy-angle correlations in neutron-emission spectra from  ${}^9\text{Be}$  reactions. For this reason we have used a special format to incorporate the  ${}^9\text{Be}(n,2n)$  data. In particular, we have derived cross sections and angular distributions for a series of (n,n') level excitation energy bins that suitably represent the Los Alamos<sup>16</sup> experimental data at 5.9, 10.1, and 14.2 MeV. Because the evaluated excitation data actually represent (n,2n) reactions, a multiplicity factor of 2 is specified in the evaluation. The level excitation functions were smoothly interpolated and extrapolated to other incident neutron energies, so that the energy range from threshold to 20 MeV is covered.

Because of the special data format used, it was necessary to modify the NJOY code to permit multigroup processing of the data. This modification is complete, and we have processed the new evaluation into the TD-Division 30-neutron by 12-gamma group structure.

J. Reevaluation of Neutron-Induced Cross Sections for  ${}^{237}\text{U}$  and  ${}^{239}\text{U}$  (R. J. Barrett, P. G. Young, and R. E. Seamon [TD-6])

The ENDL-76 evaluations of neutron-induced reactions on  ${}^{237}\text{U}$  and  ${}^{239}\text{U}$  have been revised to reflect recent nuclear-model calculations by Gardner<sup>19</sup> at Livermore and Jary<sup>20</sup> at Bruyères-le-Châtel. Below 2 MeV, the elastic (n, $\gamma$ ) and (n,f) cross sections calculated by Gardner<sup>19</sup> were included in the evaluations. At higher energies, the data were joined smoothly to the (n,f), (n,2n), and (n,3n) calculations by Jary.<sup>20</sup> Above 2 MeV, the ENDL-76 elastic, (n, $\gamma$ ), and nonelastic cross section were essentially retained, although some modification was required to accommodate in a continuous fashion both sets of model calculations. The original ENDL-76 angular and energy distributions were not modified in the

reevaluation. The new data sets have been processed through NJOY into the TD-Division 30-neutron by 12-gamma group structure and made available for use.

K. Electron and Photon Spectra Between 1 and 1000 s After a Fission Burst  
(D. G. Foster, Jr., and N. L. Whittemore)

We have begun work, under a contract from the Air Force Weapons Laboratory (AFWL), on producing a compact parameterization of the electron and photon spectra emitted between 1 and 1000 s after a fission burst. In contrast to most reactor applications, we are interested here in the particle spectrum (beta or gamma per MeV per fis/s) rather than the energy spectrum (MeV per MeV per fis/s). The sponsor's requirements include:

1. Data for  $^{235}\text{U}$ ,  $^{238}\text{U}$ , and  $^{239}\text{Pu}$  for fission and 14-MeV neutrons.
2. Moderate accuracy (5-10%).
3. Fairly detailed description (20 electron groups, 20-40 photon groups, concentrated at the lower energies).
4. Coverage of the time range from 1 to 1000 s with satisfactory extrapolation to somewhat earlier and later times.
5. Smallest feasible number of parameters (if possible, fewer than 10 per group).

In accordance with previous work,<sup>21</sup> we intend to use an exponential-series fit to the time-dependent spectrum calculated by combining data on the spectra of 180 selected fission-product nuclides with decay rates calculated using CINDER, and normalizing the composite spectrum to the calculated energy-release rate for 825 nuclides. Because the 180 nuclides were selected originally for reactor decay-heat calculations at considerably later times, the normalization exceeds a factor of 2 below 50 s.

The necessary CINDER calculations have already been done using ENDF/B-IV data for each of the required cases except  $^{239}\text{Pu}$  fission induced by 14-MeV neutrons. For the latter case we will use preliminary ENDF/B-V data as soon as they become available. All of these calculations have been performed using 50-keV groups for photons and 100-keV groups for electrons. Some of the required cases have been calculated at two time steps per decade and some at a total of seven time steps per decade. If necessary, we will use decay constants from seven/decade fits to supplement the fits at two/decade.

In preparation for the fits, we have processed the 180 standard spectra into a compact binary library using an ad hoc code SPECFL. We have also reduced all of the CINDER data to compact binary form and sorted it into the same order of

nuclides as the representative spectra, using the code CINDFL. The output from these two codes has been combined using FPSPEC, and absolute spectra for each case from 1 to  $10^{11}$  s have been stored in a working binary library. We have also prepared a streamlined version of FPSPEC that reads the normalized data back from the final library for listing, plotting, and comparing with measurements. All of the data are stored in Photostore for ready retrieval. Each step in the data preparation has been embodied in a CROS macro to simplify the processing of new data.

A primitive version of a fitting code called FPSPFT has been debugged. FPSPFT fetches the necessary data from the library, rebins it into the AFWL group structure, and carries out the required fits. The weighting function assumes a constant fractional error for all times. We make an initial fit by assuming time constants equally spaced logarithmically over the required time interval and fitting just the corresponding amplitudes (a linear problem with an exact solution). Then the fit is iterated on all parameters until it converges.

As anticipated, the initial stages of iteration frequently prove unstable. Accordingly, the code automatically reduces the step along the gradient until it gets a  $\chi^2$  smaller than the previous one. At each subsequent iteration, it attempts to double the step so that convergence is rapid after the unstable region has been crossed.

The major addition required to complete FPSPFT is a provision for automatically holding some parameters fixed if the problem is underdetermined, together with an efficient system for storing parameter sets for restarting fits or initializing new ones. The primitive version arbitrarily fixes enough of the longest time constants to make the problem exactly determinate.

## II. NUCLEAR CROSS-SECTION PROCESSING

### A. The MATXS1 Cross-Section Library (R. E. MacFarlane and D. W. Muir)

An extensive new library of neutron cross sections and scattering matrices, photon-production matrices, and photon-interaction cross sections and matrices has been generated using the NJOY processing code and ENDF/B-IV data. This library uses the standard TD-Division 30-group neutron structure and weight function and the standard 12-group gamma structure. It contains neutron cross sections for 65 nuclides, photon-production data for 41 nuclides, and photon-interaction data for 41 elements (see Table II).

TABLE II

## CONTENTS OF MATXS1 LIBRARY

<u>Neutron Interaction</u>			<u>Photon Interaction</u>		
H-1	Ca	Re-187	H	K	Cd
H-2	Ti	Au-197	He	Ca	Sn
H-3	V	Pb	Li	Ti	Ba
He-3	Cr	Th-232	Be	V	Gd
He-4	Mn-55	Pa-233	B	Cr	Ta
Li-6	Fe	U-233	C	Mn	W
Li-6a	Co-59	U-234	N	Fe	Re
Li-7	Ni	U-235	O	Co	Pt
Be-9	Cu	U-236	F	Ni	Au
B-10	Zirc2	U-237	Na	Cu	Pb
B-11	Nb-93	U-238	Mg	Zr	Th
C-12	Mo	U-239	Al	Nb	U
C-12a	Rh-103	Np-237	Si	Mo	Pu
N-14	Ag-107	Pu-238	Cl	Ag	
O-16	Ag-109	Pu-239			
F-19	Cd	Pu-240			
Na-23	Ta-181	Pu-241			
Mg	W-182	Pu-242			
Al-27	W-183	Am-241			
Si	W-184	Am-243			
Cl	W-186	Cn-244			
K	Re-185				

Photon Production

H-1	Al-27	Mo
H-2	Si	Ta-181
Li-6	Cl	W-182
Li-6a	K	W-183
Li-7	Ca	W-184
Be-9	Ti	W-186
B-10	V	Pb
C-12	Cr	U-235
C-12a	Mn-55	U-237
N-14	Fe	U-238
O-16	Co-59	U-239
F-19	Ni	Pu-240
Mg	Nb-93	

The library is available in the new MATXS format that allows for the storage of all data types and partial cross sections in a compact manner. The data can be reformatted for use in existing transport codes using the TRANSX program described in Sec. II.B.

ENDF/B-IV cross sections were reconstructed to an accuracy of 0.5% and Doppler broadened to 300 K. Multigroup averages were computed at infinite dilution. Heat-production cross sections (eV b) are included for both neutron and photon interactions. Neutron heating for isotopes without photon-production data was calculated by assuming that all photon energy is deposited locally. Photon form factors were used in generating the photon interaction data, therefore low-energy cross sections and coherent scattering anisotropy should be better than for older methods.

This library contains all the group constants required for coupled neutron, photon, heating, and sensitivity calculations where self-shielding is not important.

#### B. TRANSX (R. E. MacFarlane)

As reported above, we have prepared a rather complete cross-section library with 30 neutron groups and 12 photon groups in the new MATXS format. This library has neutron interaction data (including heating cross sections) for 65 nuclides, photon-production data for 41 nuclides, and photon-interaction data (including heating) for 41 elements. All necessary data is present for complete coupled neutron, photon, and heating calculations when self-shielding is not important. However, this extensive new library is of little use unless its contents can be delivered to the existing transport codes in a convenient way. TRANSX is a code written for this purpose.

TRANSX allows the user to construct neutron tables, photon tables, or coupled sets. The tables can be produced in "matwise" ordering (i.e., MAT1 P<sub>0</sub>, MAT1 P<sub>1</sub>, ..., MAT2 P<sub>0</sub>, ..., etc.) that can be read by almost all existing transport codes, or the user can specify "groupwise" ordering. This is the format used internally by all DTF-like codes, and it allows problems to be run with many groups. The tables can be generated in adjoint form if desired. TRANSX also allows for transport corrections, for prompt or infinite time fission parameters, for collapse to a subset group structure, and for the creation of microscopic or macroscopic mixtures.

Finally, TRANSX can be used to construct sophisticated edit cross sections. The MATXS file allows for all the partial cross sections found on the original ENDF/B files plus others, such as heating, constructed by the processing code. The TRANSX user can construct any edit that is a linear combination of vector partials from the MATXS file. Some examples may help to make this clear.

Example 1.  $^{12}\text{C}$  (ENDF/B MAT1274)

$$^4\text{He production} = 1 * (n, \alpha) + 3 * (n, n'3\alpha)$$

Example 2.  $n + ^7\text{Li} \rightarrow ^8\text{Li} \rightarrow e^- + 2\alpha$  (850 ms)

$$\text{total heating (eV b)} = 1 * (\text{prompt heating}) + 9.31 \times 10^6 * (n, \gamma)$$

The quantities in parentheses are available on the MATXS file. Special options are included for fission chi and for edits of gamma production sources, including delayed gammas.

TRANSX uses variable-dimensioning and paging throughout. There is essentially no limit on the size of a problem that can be run.

### C. Collapse Theory (D. W. Muir and R. E. MacFarlane)

We have modified the CINX code to perform space-energy collapse with a full Legendre treatment. To discuss the theory behind the new collapsing algorithms, we introduce the following notation:

- v = volume of a spatial region
- n = density of the nuclide of interest
- $\sigma$  = cross section for reaction of interest
- $\phi$  = neutron fluence
- l = Legendre expansion order
- g = fine-group index
- G = coarse-group index
- k = fine-mesh index
- K = coarse-mesh index

Let us repeat the usual argument for preserving the reaction rate integrated over some finite region of both space and energy.

$$\left. \begin{matrix} R \\ G \end{matrix} \right|_{\text{fine}} = \sum_{k \in K} \sum_{g \in G} n^k \sigma_g^k \phi_g^k v^k$$

Since an integration over angle has already been performed, only the scalar flux

$$\phi_{0g}^k = \phi_{\ell g}^k |_{\ell 0}$$

is required. Further

$$R_G^K \Big|_{\text{coarse}} = \sum_{k \in K} \sum_{g \in G} n^k \sigma_G^K \phi_{0g}^k$$

Setting the two reaction rates equal to one another and dividing through, we have

$$\sigma_G^K = \frac{\sum_{g \in G} \sigma_g \phi_{0g}^k}{\sum_{g \in G} \phi_{0g}^k} \quad (1a)$$

where

$$\phi_{0g}^k = \sum_{k \in K} n^k \phi_{0g}^k \quad (1b)$$

is the volume-integrated scalar flux in the coarse-mesh region K. This result is identical to the usual result for scalar-flux collapse, except for our slight generalization to allow for the fact that the atomic density  $n^k$  may vary as a function of fine-mesh interval.

The collapsing algorithm, Eq. (1), allows us to define an equivalent average cross section  $\sigma_G^k$  that is constant within a coarse-mesh spatial interval and within a coarse energy group. This constant cross section gives the same result as the detailed cross section  $\sigma_g$  in calculations of reaction rates using the same fine-group flux. Since, to a good approximation, the sum of the fine-group fluxes within a coarse group will be equal to the flux in that coarse group calculated in a coarse-group calculation, we have the desired result that the reaction rate is preserved in going from an entirely fine-group calculation to an entirely coarse-group calculation.

Under the phrase "reaction rates" above, we include flux integrals of any angle-integrated cross section, including individual members of the  $P_0$  coarse-group transfer matrix,  $\sigma_{0;G \rightarrow G'}^K$ . In other words, the total number of neutrons in region K undergoing the particular transition from group G to group G' is preserved. However, it should be noted at this point that the angular distribution of these scattered neutrons is not necessarily preserved by the collapse algorithm given in Eq. (1), since we have dealt only with angle-integrated quantities. Fortunately, to conserve the neutron scattering angular distributions, only a slight extension of the above concepts is required.

Let  $S_{G \rightarrow G'}^K(\mu)$  be the volume integrated angular distribution of neutrons being scattered from source energy group G to sink group G', i.e., the scattering "source" term in the Boltzmann equation. From Ref. 22 the  $\ell$ -th Legendre moment of the scattering source is just

$$S_{\ell;G \rightarrow G'}^K \Big|_{\text{fine}} = \sum_{k \in K} \sum_{g \in G} \sum_{g' \in G'} n^k \sigma_{\ell;g \rightarrow g'}^k \phi_{\ell g}^k v^k$$

in the fine-group environment, and

$$S_{\ell;G \rightarrow G'}^K \Big|_{\text{coarse}} = \sum_{k \in K} \sum_{g \in G} n^k \sigma_{\ell;G \rightarrow G'}^k \phi_{\ell g}^k v^k$$

in the coarse-group environment. We can preserve  $S_{G \rightarrow G'}^K(\mu)$  by preserving its Legendre moments; so we proceed as before, setting the two expressions above equal to one another and solving for  $\sigma_{\ell;G \rightarrow G'}^K$ .

$$\sigma_{\ell;G \rightarrow G'}^K = \frac{\sum_{g \in G} \sigma_{\ell;g \rightarrow G'}^k \phi_{\ell g}^k}{\sum_{g \in G} \phi_{\ell g}^k} \quad (2a)$$

where

$$\sigma_{\ell;g \rightarrow G'} = \sum_{g' \in G'} \sigma_{\ell;g \rightarrow g'} \quad (2b)$$

and

$$\phi_{\ell g}^K = \sum_{k \in K} n^k \phi_{\ell g}^k v^k \quad (2c)$$

Thus, the  $\ell$ -th Legendre moment of the angular flux should be used to collapse the  $\ell$ -th Legendre moment of the cross sections, in a manner completely analogous to the use of the scalar flux to collapse angle-integrated cross sections.

#### D. PCS Calculations (E. B. Kidman)

The Processing Code Subcommittee of the Code Evaluation Working Group has specified a simple reactor system that can be used to test and compare various code systems. As results from the various labs arrive, a number of possible errors and unifying actions begin to take shape.

Instead of using, from the beginning, an arbitrary fission source to avoid a possible source of discrepancies, it appears either the various code systems are not flexible enough to accept an arbitrary fission source or the various lab participants prefer to compare their sundry schemes for computing a realistic fission source for this fictitious reactor system. Thus, in an effort to make the final results more uniform, the LASL calculations have been repeated using a more composition-reflective fission source. The results are shown in Table III. Still, however, the NEW LASL CHI is not the same as the ANL CHI. If the NEW LASL CHI is substituted for the ANL CHI or vice versa, the ANL CHI yields a lower  $K_{\infty}$  by 0.0007. Thus there is only  $1.2121 - 1.2096 - 0.0007 = 0.0018 \Delta K$  left to be explained between the LASL and ANL results for the  $B^2 = 0$  problem.

New schemes for generating effective elastic removal cross sections could have an effect on the LASL PCS eigenvalues. (See Sec. II.E on Elastic Removal Schemes.) Adoption of an improved scheme could raise the LASL PCS  $B^2 = 0$  eigenvalues by 0.0082, and the LASL PCS  $B^2 = 0.00073$  eigenvalues by 0.0044. This would diminish the extent of agreement among the various labs.

TABLE III

## FISSION SOURCE EFFECTS

<u>Lab</u>	<u>Codes</u>	<u>Comments</u>	<u>PCS System With</u>	
			<u>B<sup>2</sup>=0</u>	<u>B<sup>2</sup>=0,00073</u>
LASL	MINX/1DX	LIB-IV, new LASL CHI	1.2121	1.0061
LASL	MINX/1DX	LIB-IV, old LASL CHI	1.2140	1.0077
LASL	ETOX/1DX	ETOX-IV, new LASL CHI	1.2108	1.0053
LASL	ETOX/1DX	ETOX-IV, old LASL CHI	1.2127	1.0069
ANL	ETOE/MC2-II/SDX		1.2096	

Finally, some confusion exists as to what cross sections and f-factors should be used in the iteration to obtain  $\sigma_0$ , the background cross section. The effective total cross section should be used in the  $\sigma_0$ -iteration. In 1DX,<sup>23</sup> this is accomplished by simply using the infinitely dilute total cross section in the first iteration, while subsequent iterations form an effective total cross section from the infinitely dilute fission, capture, elastic, and inelastic cross sections and their f-factors. The "total f-factor," FTOT, provided by LIB-IV<sup>24</sup> is not used because it is a current weighted entity that would yield an improper total cross section for use in the  $\sigma_0$ -iteration. However, if this improper method were used, it would increase the  $B^2 = 0$  PCS eigenvalues by 0.0008.

#### E. Elastic Removal Schemes (R. B. Kidman)

Effective elastic removal cross sections are sensitive to problem-dependent intragroup spectra. Iterative procedures between flux and elastic removal cross sections have shown promise for adjusting these cross sections to the problem-dependent spectra. However, since more accurate elastic removal cross sections have become available, it is appropriate to consider improving the nature of the interpolations involved in the iteration process.

Table IV shows the results of using three different schemes on several critical assemblies. The Collision Density Scheme utilizes linear interpolation on the collision density to determine ratios that modify the elastic removal cross sections. The Higher Order Scheme utilizes polynomial approximations to the current cross section and flux trends, and performs group averaging integrals to determine ratios that modify the elastic removal cross section.

The original 1DX scheme develops elastic removal cross sections much different than the original cross sections provided by LIB-IV. Since the original LIB-IV elastic removal cross sections are very realistic, any large deviations

TABLE IV  
COMPARISON OF ELASTIC REMOVAL SCHEMES

	<u>Original LDX Scheme</u>	<u>Collision Density Scheme</u>	<u>Higher Order Scheme</u>
<u>PCS (B2=0.0)</u>			
K after 0 iterations	1.22676	1.22676	1.22676
K after 5 iterations	1.21405	1.21912	1.22227
K0 - K5	0.01271	0.00764	0.00449
New K5 - LDX K5		0.00507	0.00822
<u>PCS (B2=0.00073)</u>			
K after 0 iterations	1.01615	1.01615	1.01615
K after 5 iterations	1.00773	1.00980	1.01216
K0 - K5	0.00842	0.00635	0.00399
New K5 - LDX K5		0.00207	0.00443
<u>ZPR-6-7</u>			
K after 0 iterations	0.97921	0.97921	0.97921
K after 5 iterations	0.97085	0.97290	0.97520
K0 - K5	0.00836	0.00631	0.00401
New K5 - LDX K5		0.00205	0.00435
<u>ZPR-3-54</u>			
K after 0 iterations	0.92590	0.92590	0.92590
K after 5 iterations	0.93222	0.92518	0.92345
K0 - K5	-0.00632	0.00072	0.00245
New K5 - LDX K5		-0.00704	-0.00877

are suspicious. Since the 0<sup>th</sup> iteration uses the original cross sections, the 0<sup>th</sup> iteration eigenvalue represents a valid alternative to the original LDX procedure. This is why the 0<sup>th</sup> iteration eigenvalue is listed in Table IV.

We are now formulating evaluation criteria which will allow us to determine which scheme would be most appropriate to adopt.

#### F. Elastic Removal F-Factor Effects (R. B. Kidman)

Past applications of the Shielding Factor Method did not utilize actual elastic removal f-factors to help determine the effective elastic removal cross section. Instead, the elastic f-factor was used.

The LDX code has been modified to use actual elastic removal f-factors. Preliminary effects of factoring in only iron elastic removal f-factors are shown

in Table V. (These 1DX runs also contain the Higher Order Elastic Iteration Schemes mentioned in the section on Elastic Removal Schemes.) In Table V,  $F_d$  refers to elastic removal f-factors and  $F_e$  refers to elastic f-factors. Since ZPR-3-54 was an iron-dominated reflector, there is a large effect. Since the infinite homogeneous PCS  $B^2 = 0$  system has no leakage and is not dominated by iron, the effect is very much smaller.

Before these results can be taken seriously, the  $\sigma_0$ -behavior of elastic removal f-factors will have to be investigated to determine if a more generalized  $\sigma_0$ -interpolation of f-factors is required.

G. Space-Shielding Cross Sections for Pebble-Bed High-Temperature Reactors  
(M. G. Stamatelatos and R. J. LaBauve)

New methods to space shield group cross sections for use in Pebble-Bed High-Temperature Reactor (PBHTR) calculations have been developed. These represent modifications of methods developed and successfully used in analyses of High-Temperature Gas-Cooled Reactors (HTGR). Important modifications of the original methods were required by the geometric peculiarities of PBHTR systems of German design whose fuel elements are tightly packed spheres having an inner mixture of graphite and fine grains and an outer graphite spherical shell. This material is the basis for a presentation at the American Nuclear Society's Annual Meeting in New York in June.

H. Pointwise Cross-Section Space Shielding in Doubly Heterogeneous Reactors  
(M. G. Stamatelatos and R. J. LaBauve)

A number of methods have been developed or implemented at LASL for calculating space-shielded cross sections for double-heterogeneous HTGR systems.<sup>25-27</sup> A new method is currently being investigated for space-shielding cross sections of such HTGR systems at the pointwise or ultrafine energy level. Preliminary

TABLE V

ELASTIC REMOVAL F-FACTOR EFFECTS

Critical Assembly	$K_\infty$	$K_\infty$ Actual Iron $F_d$	$\Delta K$
	All $F_d = F_e$	Others $F_d = F_e$	
ZPR-3-54	0.92345	0.92803	0.00458
PCS $B^2 = 0$	1.22227	1.22257	0.00030

results have been satisfactory, and comparisons with other methods are in progress. A full description of the method and the results it produces will be given in a future report.

I. Cross Sections for HTGR Safety Research (M. G. Stamatelatos and R. J. LaBauve)

Our report titled "Methods for Calculating Group Cross Sections for Doubly Heterogeneous Thermal Reactor Systems," LA-NUREG-6685-MS, was recently published (February 1977). It discusses methods used at LASL for calculating group cross sections in doubly heterogeneous HTGR systems of the General Atomic design. These cross sections have been used for neutronic safety analysis calculations of such HTGR systems at different points in reactor lifetime (e.g., beginning-of-life, end-of-equilibrium cycle).

III. CONSISTENCY ANALYSIS OF DIFFERENTIAL AND INTEGRAL NEUTRONICS DATA: THERMONUCLEAR TRITIUM PRODUCTION (W. A. Reupke [Georgia Institute of Technology] and D. W. Muir)

In previous reports<sup>28-32</sup> we have documented the development of least squares consistency analysis methods and have illustrated the method by preliminary application to a 14 MeV neutron-driven tritium production integral experiment.<sup>33</sup> Using the code ALVIN we have now evaluated the consistency of the data prior to and after statistical data adjustment. The experimental tritium production in  ${}^6\text{Li}$  (natural abundance) and  ${}^7\text{Li}$  detectors, imbedded in a 30-cm-radius  ${}^6\text{LiD}$  sphere, is shown in Fig. 9. The standard derivations of the integral data, indicated by the vertical bars, correspond to the trace of the full dispersion (error) matrix shown in Fig. 10. Here detector positions are indexed in order of increasing radius and the error matrix elements are presented as fractional, or relative, variance-covariance units.

A perturbation calculation of the tritium-production cross-section sensitivities was performed, using a development of the ALVIN sensitivity calculation module SENSI, with secondary neutron energy and angular distributions held constant. The resulting multigroup sensitivity matrix is shown in Fig. 11.

When the multigroup sensitivity matrix is folded with a cross section dispersion matrix using a generalized law of propagation of errors, it is then possible to bound the calculated tritium production with error bars that represent that part of the uncertainty in the calculated production due to the cross-section uncertainty. The dispersion matrices of the most important

partial reactions in this experiment were evaluated by criteria of external consistency. The bulk of the uncertainty in calculated tritium production was found to be due to the  ${}^7\text{Li}(n,xt)$  reaction. The dispersion matrix of the multigrouped reactions (Fig. 12), as implemented in a separate ALVIN run, is shown in Fig. 13. The resulting uncertainty bands of the calculated tritium production, obtained by folding the sensitivity matrix of Fig. 11 with the error matrix of Fig. 13, is shown in the form of dotted lines in Fig. 9.

Statistical adjustment of the combined data, with an initial chi-square per degree of freedom ( $\chi^2/\text{DF}$ ) of 3.0, leads to a final  $\chi^2/\text{DF}$  of 2.3, and represents a fifteenfold improvement in statistical likelihood. The detailed pattern of adjustment is indicated by the solid lines in Figs. 9 and 12. Note that the improvement is achieved by a decrease in the  ${}^7\text{Li}(n,xt)$  14-MeV group cross section from 328 to 284 mb and an adjustment of the  ${}^6\text{Li}$  data closer to calculated values. The adjusted  ${}^7\text{Li}(n,xt)$  cross-section dispersion matrix and the adjusted tritium-production dispersion matrix are shown in Figs. 14 and 15. The correlations between adjusted cross-section data and adjusted tritium production data are shown in Fig. 16. No correlations were assumed between the errors of the

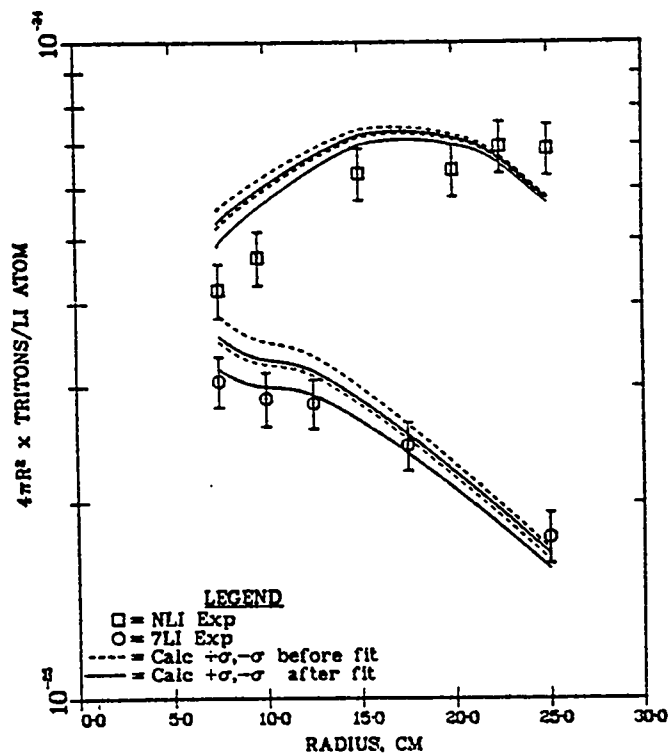


Fig. 9.

Radial tritium production before and after fit. Initial  $\chi^2/\text{DOF} = 2.3$  (combined data).

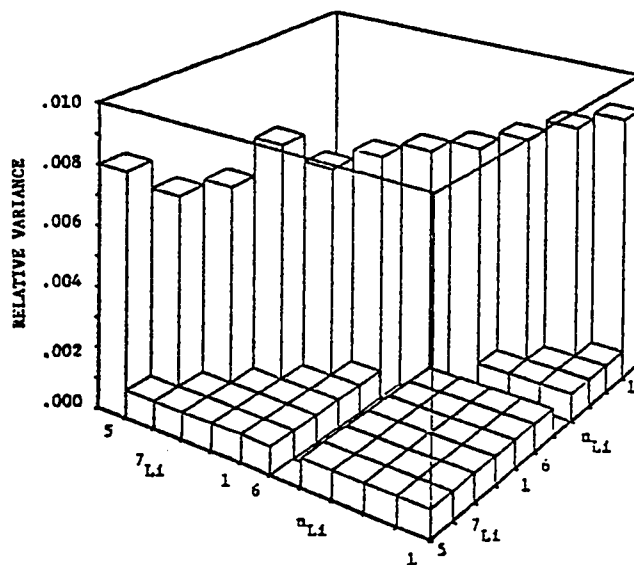


Fig. 10.

Tritium production relative dispersion matrix, before adjustment.

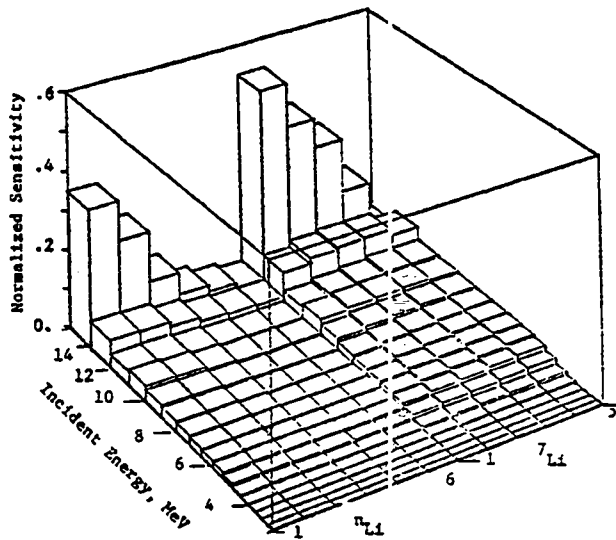


Fig. 11.  
Multigroup sensitivity matrix,  ${}^7\text{Li}$  (n,xt) reaction. Total cross-section constant.

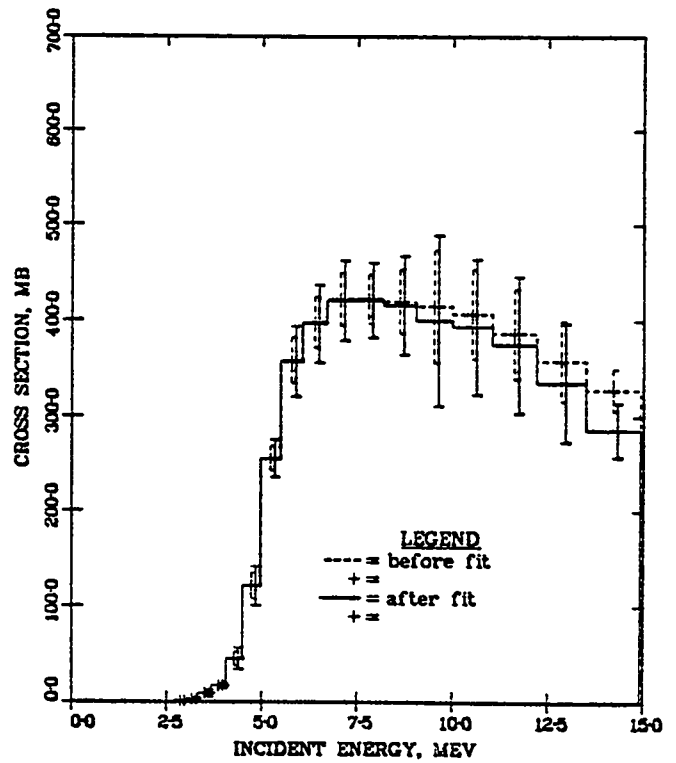


Fig. 12.  
 ${}^7\text{Li}$ (n,xt) group cross sections before and after fit. Initial  $\chi^2/\text{DOF} = 3.0$ , final  $\chi^2/\text{DOF} = 2.3$  (combined data).

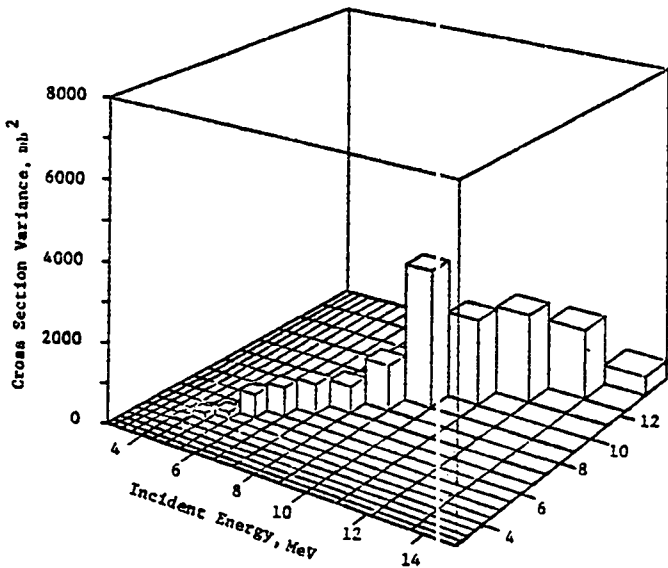


Fig. 13.  
 ${}^7\text{Li}$ (n,xt) reaction, multigroup dispersion matrix, before adjustment.

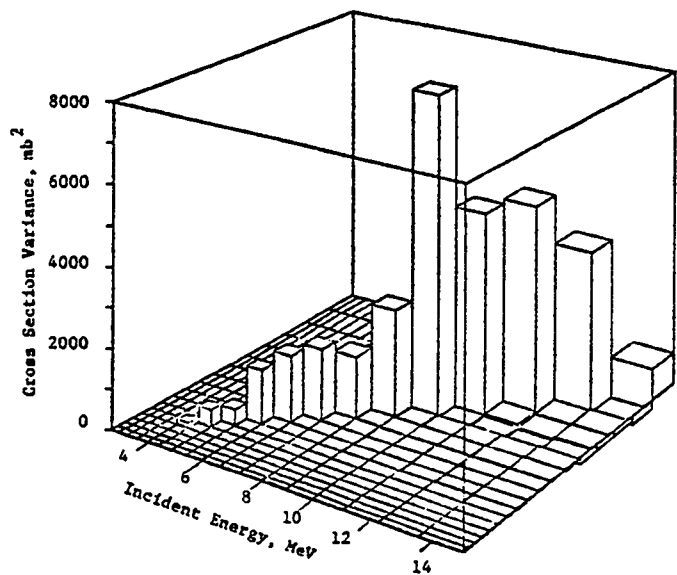


Fig. 14.  
 ${}^7\text{Li}$ (n,xt) reaction, multigroup dispersion matrix, after adjustment.

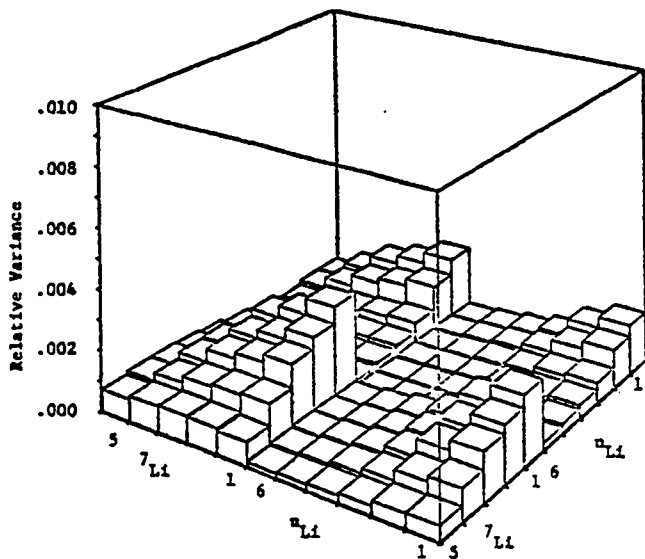


Fig. 15.  
Tritium production dispersion matrix,  
after consistency analysis.

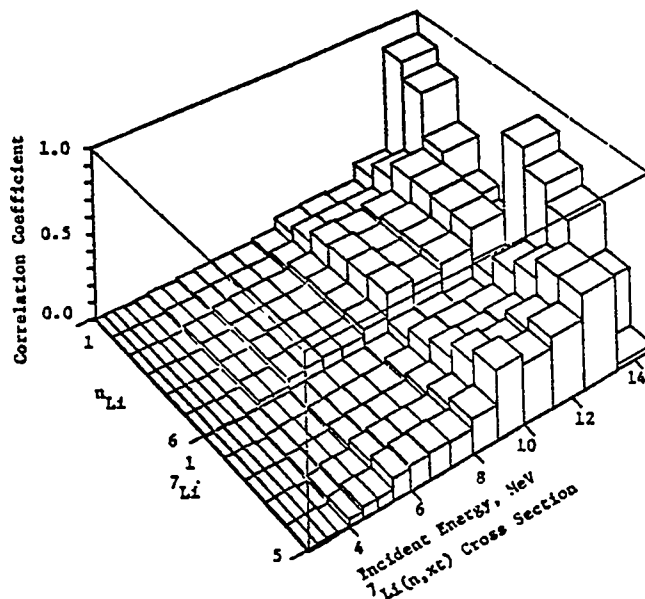


Fig. 16.  
Correlation coefficient matrix, after  
adjustment.

initial cross-section data as a type and the initial integral data as a type. Using the adjusted data, the uncertainty in the tritium breeding ratio in pure  ${}^7\text{LiD}$  is reduced by one-fifth.

A complete discussion of the method and results is found in Ref. 34. Grateful acknowledgment is extended to M. L. Prueitt for making available the code PICTURA used in preparing the graphics.

#### IV. FISSION-PRODUCT, ACTINIDE, AND DECAY DATA

A. Fission Yield Theory (D. G. Madland, R. E. Pepping [University of Wisconsin], C. W. Maynard [University of Wisconsin], T. R. England, and P. G. Young)

Fission-fragment yields for  ${}^{235}\text{U}$  thermal fission have been calculated using a simple Fermi gas model for the fragment level densities. The calculation has been performed for three cases. In Case A, the primary fragments are assumed to be produced in their ground-state shapes; in Case B, the fragments are allowed to deform, but the shapes are assumed to be those corresponding to the maximum value of the G-function, described below; and in Case C, an integration is performed over the allowed shape space.

According to the statistical assumption, the yield of a fragment pair Y in a given shape configuration is proportional to the double integral,

$$Y(\epsilon) \propto \int_0^{G(\epsilon)} \rho(k) \int_0^{G-k} \omega_1(E_1) \omega_2(E-E_1) dE_1 dk$$

Here  $\omega_1$  is the nuclear level density of the  $i^{\text{th}}$  fragment,  $E$  is the total energy partitioned to fragment internal degrees-of-freedom,  $\rho$  is the density of translational states, and  $k$  is the pre-scission kinetic energy. The quantity  $G$  is the energy release at scission and is given by

$$G(\epsilon) = E + k = M^* - m_1(\epsilon^{(1)}) - m_2(\epsilon^{(2)}) - C(\epsilon^{(1)}, \epsilon^{(2)}, \delta)$$

where  $M^*$  is the mass of the fissioning compound nucleus,  $m_1$  is the mass of the  $i^{\text{th}}$  fragment characterized by Nilsson deformation parameters  $\epsilon^{(i)}$  and  $\epsilon_4^{(i)}$ , and  $C$  is the Coulomb repulsion energy at scission as given by the formulation of Hirschfelder et al.<sup>35</sup> In order to insure that  $G > 0$ , a parameter  $\delta$  must be included in the Coulomb energy expression. This parameter may be interpreted as the separation between fragment charge distributions at scission, i.e., the fragment charge distributions are apparently not tangent at scission. The pre-scission kinetic energy, in the assumed model, is a small, slowly varying function of  $G$  and a magnitude of the order of a few MeV.  $G$  and  $E = G - k$  are then essentially the same and exhibit the same systematic behavior.

Fragment masses are computed from the formula of Seeger and Howard.<sup>36</sup> Binding energies are computed on a grid of 20 values of  $\epsilon$  (the Nilsson quadrupole deformation parameter) and 5 values of  $\epsilon_4$  (the hexadecapole deformation parameter). To simplify computations, we have chosen to vary  $\epsilon$  and hold  $\epsilon_4$  fixed at approximately the most probable value for a given  $\epsilon$ . Thus, a fragment may be formed in 1 of 20 possible shapes. For a given fragment pair, there are 400 possible combinations of fragment shapes. The  $G$ -function is evaluated for each combination.

For the purpose of illustration, we have calculated yields for values of 4.5 and 6.4 F. Our results are shown in Figs. 17-20. In case A, where the fragment shapes are assumed to be those of the ground-state, a strong minimum occurs in the vicinity of light fragment mass 95 (Figs. 17 and 18). We have shown this to result from a rather abrupt decrease in the average charge separation between the fragments in this region. This causes an increase in the Coulomb term and a corresponding decrease in  $G$  and  $E$ . In the simple Fermi gas

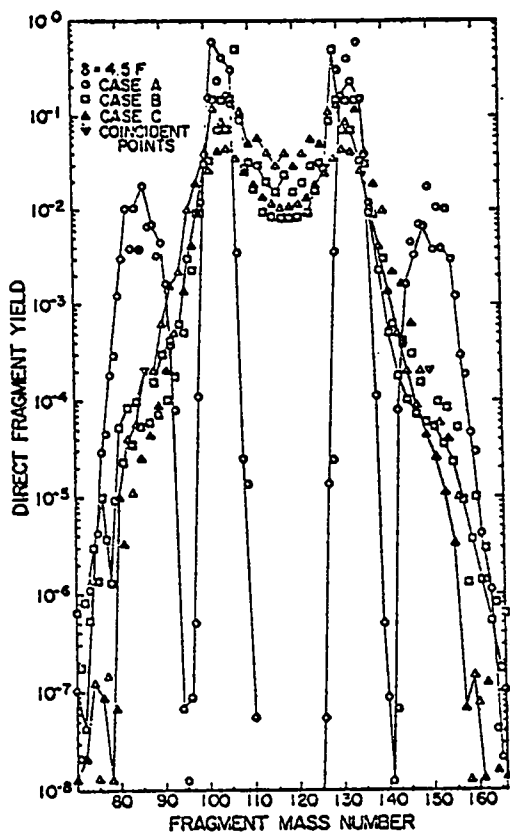


Fig. 17.

Fission fragment mass chain yields in  $^{235}\text{U}$  thermal fission as a function of mass number for  $\delta = 4.5 \text{ F}$ . The lines are drawn through even mass numbers for  $A \leq 118$  and through odd mass numbers for  $A \geq 119$ .

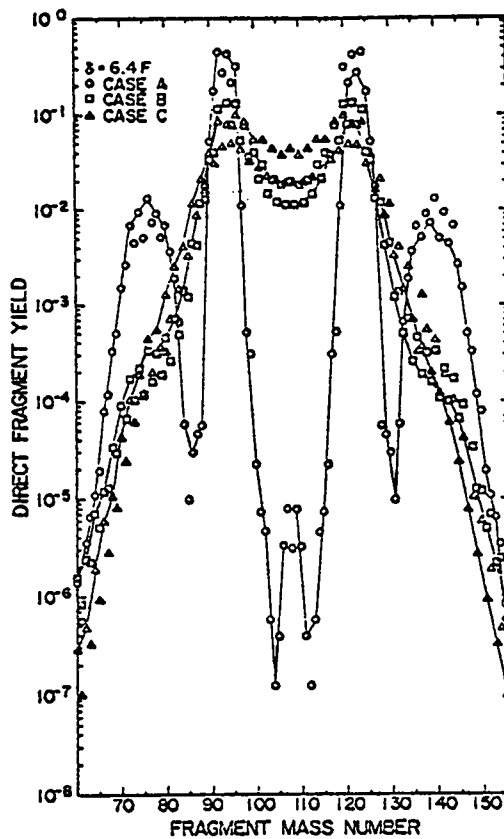


Fig. 18.

Fission fragment mass chain yields in  $^{235}\text{U}$  fission as a function of mass number for  $\delta = 6.4 \text{ F}$ . The lines are drawn through even mass numbers for  $A \leq 118$  and through odd numbers for  $A \geq 119$ . The abscissa has been mislabeled, i.e., "70" should be "80," and "80" should be "90," etc.

model of nuclear level densities, the yield expression is essentially an exponential in  $E^{1/2}$ . The yield itself is then topologically similar to the G and E functions. In Case B, the fragments are assumed to have shapes corresponding to the combination that gives maximum values of G for this configuration. In Case C, the yield is computed at all 400 points and the result integrated over the grid,  $\epsilon^{(1)} \times \epsilon^{(2)}$ . The nonphysical minimum at mass 95 is removed (in Cases B and C) by allowing fragment deformations different from those of the ground-state (Case A). In these cases, however, the inadequacies of the assumed model are still apparent. The yield peak positions and the peak-to-valley ratios do not agree well with experimental observation.<sup>37</sup>

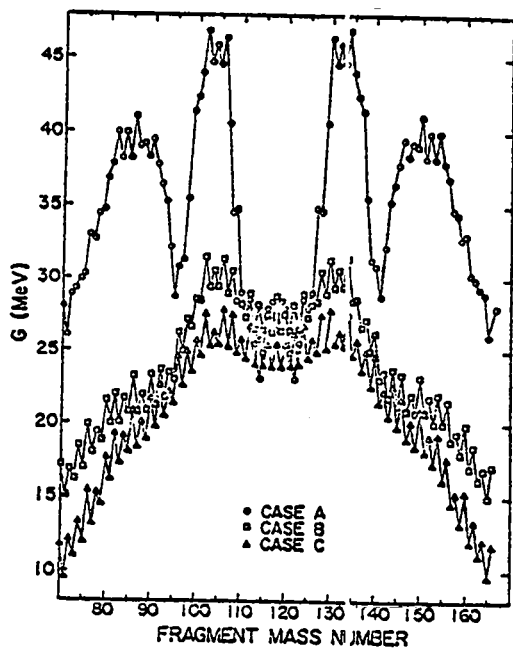


Fig. 19

The energy release at scission  $G$  in  $^{235}\text{U}$  thermal fission as a function of fragment mass number for the three cases discussed in the text.

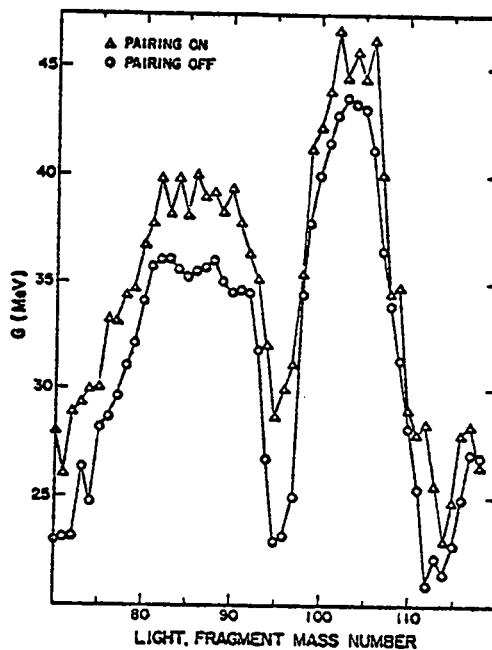


Fig. 20.

The effect on  $G$  of switching on and off the pairing contribution to the Strutinsky correction in the mass formula. The observed "smoothing" achieved by switching off the pairing is observed in all cases shown in Fig. 19.

In Fig. 19, the  $G$ -function is shown for the three cases ( $G$  is weighted by the calculated fractional independent yield to remove the  $Z$ -dependence). The curves shown are for a value of the separation parameter,  $\delta$ , of 6.4 F.

One point is noteworthy in all cases of Figs. 17-19: the  $G$ -function and yields are enhanced for even-even mass splits. It is suggested<sup>38</sup> that the pairing interaction term should be removed from the  $G$ -function by ignoring it in the fragment mass calculation. This may be done by simply ignoring the pairing contribution to the Strutinsky correction term in the mass calculation.<sup>35</sup> The effect on the  $G$ -function is shown in Fig. 20 for Case A.

The next step in the yield calculation is the use of a more sophisticated fragment level-density function such as that recommended by Gilbert and Cameron.<sup>38</sup> While still based on the Fermi gas model, shell effects in the fragments may be introduced. The pertinent quantity is available from the Strutinsky correction used in the nuclear mass formula of Seeger and Howard.<sup>36</sup>

## B. ENDF/B Phenomenological Yield Model Improvements

1. Zp Values for Neutron-Induced Fission (D. G. Madland and R. E. Pepping [University of Wisconsin]). Work is continuing on the calculation described in the previous quarterly progress report. The remaining problem still persists, that is, how to fold the effects of the prompt neutron distribution in Zp values calculated for fission fragments so as to yield Zp values for fission products. The simplest approach is to ignore the distinction between fragments and products, a process which is too inaccurate (~0.5 charge units maximum error) for many applications. The next order of approach (now being pursued) is to utilize the "saw-tooth" prompt neutron distribution  $\nu(A)$  due to Terrell<sup>39</sup> to perform an average over Z for each fixed value of A.

2. Ternary Fission Probabilities and Charge Distributions (D. G. Madland and L. Stewart). A survey has been made of experimental information pertinent to the probability of ternary fission and the charge distribution of the light-ternary-fission products. This work was performed at the request of the Fission Product and Actinide Data Subcommittee of CSEWG.

A new prescription has been formulated for the ternary fission probability as a function of the incident particle energy and certain compound nucleus properties. Based upon systematics, a method for obtaining charge distributions of light ternary products has been derived.

This work is completed and has been documented.<sup>40</sup>

## C. Short-Irradiation Fission-Product Beta Spectra and Total Energy Calculations Versus Experiment (M. G. Stamatelatos and T. R. England)

Comparisons of calculated and experimental beta spectra and total beta energy from fission-product decay following short (0.015-100 s) thermal-neutron irradiations of <sup>235</sup>U samples have been made. Experimental results from the University of Illinois<sup>41</sup> and published preliminary results from the Oak Ridge National Laboratory<sup>42</sup> benchmark experiments on fission-product decay heating were used. Calculations are based on ENDF/B-IV data.<sup>43</sup>

The beta spectra were computed in a 75-group 100 keV fixed grid structure.<sup>44</sup> Short irradiation and cooling time comparisons are stringent tests of the ENDF/B-IV data used. The good agreement between calculations and experiments in both beta spectra and total beta energies indicates that the ENDF/B-IV fission-product data are adequate for even short irradiation and cooling times and can

serve as a reliable data base for predicting delayed fission-product beta energy release under reactor accident conditions.

This material is the basis for a presentation at the American Nuclear Society's Annual Meeting in New York in June 1977.

D. Analytic Fitting of Summation Calculations of Delayed Energy Spectra from Fission Products (R. J. LaBauve, T. R. England, and M. G. Stamatelatos)

Summation calculations of delayed energy spectra from fission products can be analytically approximated by a linear combination of functions

$$f_c(t) = \sum_{k=1}^h \alpha_{kl} e^{-\lambda_k T} .$$

We have recently made single- and two-parameter fits to these functions, that is, both by (1) specifying the  $\lambda_k$ 's and fitting the  $\alpha_k$ 's<sup>45</sup> and (2) by fitting the  $\alpha_k$ 's and  $\lambda_k$ 's simultaneously.<sup>46</sup>

The advantage of the first method is rapid calculation, but with a resulting accuracy in the fit of only several percent. The second method provides a high degree of accuracy (to within tenths of a percent), but the problems require longer running times on the CDC 7600.

We have now combined the two methods in a fashion so that the preliminary results from the first method are directly applied as a first guess input to the second method with the result of greatly reducing the problem running time, without loss of accuracy. The fits for use in the ANS 5.1 Decay Heat Standard are described in the next section (Sec. IV.E).

E. Decay Heat Standard ANS 5.1 (T. R. England, M. G. Stamatelatos, R. J. LaBauve, R. E. Schenter (Hanford Engineering Development Lab), and F. Schmittroth (Hanford Engineering Development Lab))

In March the ANS 5.1 Decay Heat Working Group formally approved the decay heat power and uncertainties recommended by a joint LASL/HEDL effort. Decay heat for <sup>235</sup>U and <sup>239</sup>Pu thermal fission and <sup>238</sup>U fast fission is to be included in the standard.

The <sup>235</sup>U value is based on a generalized least square analysis<sup>21</sup> combining calculations using ENDF/B-IV data and four recent benchmark experiments: Yarnell

and Bendt at Los Alamos Scientific Laboratory; Dickens et al. at Oak Ridge National Laboratory; Lott et al. at Fontenay-aux-Roses, France; and Friesenhahn et al. at Intelcom Rad Tech. The  $^{238}\text{U}$  and  $^{239}\text{Pu}$  heating rates are based entirely on calculations using ENDF/B-IV data as corrected in Ref. 43.

The proposed standard consists of heating values following a fission pulse and an infinite irradiation (defined for practical purposes as  $10^{13}$  s) at constant power, without depletion or absorption effects. Either the pulse or infinite values can be used to generate the rates for finite irradiations. In addition, the effects of neutron absorption on heating, which is 2nd order for cooling times  $\leq 10^6$  s, is accounted for by use of an approximate expression based on earlier calculational studies.<sup>47</sup>

In the standard, tabular values for the pulse and infinite cases are given at 6 points per cooling decade, beginning at 1 s and extending to  $10^9$  s ( $10^{13}$  s for the pulse). In addition to the tabular data, it has been shown that it is possible to generate finite and infinite irradiation cases using a 2 parameter per function fit to 23 exponentials:

$$f(t) = \sum_{i=1}^{23} f_i e^{-\lambda_i t} \quad \text{MeV/Fiss-s}$$

$$F(t,T) = \sum_{i=1}^{23} f_i e^{-\lambda_i t} (1 - e^{-\lambda_i T}) \quad \text{MeV/Fiss} \quad ,$$

where

t = cooling time in seconds

T = irradiation time in seconds.

The latter expression F(t,T) applies to a constant fission rate over the interval T and, as described in the ANS 5.1 Standard, the f(t) functions can be readily folded into any variable fission rate.

Because of the accuracy of these fits, the tabular data will be generated directly from them. Tables VI-VIII provide the final recommended parameters.

TABLE VI

PARAMETERS FOR  $^{235}\text{U}$  THERMAL FISSION FUNCTIONS  $f(t)$  AND  $F(t, \infty)$ <sup>a</sup>

$\alpha$	$\lambda$	$\alpha$	$\lambda$
6.4447E-1	7.8950E+0	2.5441E-6	9.9966E-6
4.6408E-1	5.5683E-1	4.9828E-7	2.5405E-6
2.8883E-1	2.2367E-1	1.8522E-7	6.6349E-7
1.4815E-1	1.0212E-1	2.6606E-8	1.2289E-7
5.5143E-2	3.3400E-2	2.2397E-9	2.7212E-8
2.1950E-2	1.1403E-2	8.1609E-12	4.3701E-9
3.1497E-3	3.2092E-3	8.7797E-11	7.5780E-10
6.7681E-4	1.3098E-3	2.5129E-14	2.4786E-10
8.3288E-4	6.4795E-4	3.2190E-16	2.2376E-13
2.0207E-4	2.0059E-4	4.4911E-17	2.4499E-14
3.7154E-5	6.0023E-5	7.4776E-17	1.5643E-14
8.5033E-6	2.1715E-5		

$$a \quad f(t) = \sum_{i=1}^{23} \alpha_i e^{-\lambda_i t} \quad \text{MeV/Fission-s}$$

$$F(t, T) = \sum_{i=1}^{23} \frac{\alpha_i}{\lambda_i} e^{-\lambda_i t} (1 - e^{-\lambda_i T}) \quad \text{MeV/Fission}$$

$$F(t, \infty) \equiv F(t, 10^{13})$$

t and T in seconds

b

Read as  $6.4447 \times 10^{-1}$

TABLE VII

PARAMETERS FOR  $^{238}\text{U}$  FAST FISSION FUNCTIONS  $f(t)$  AND  $F(t, \infty)$ <sup>a</sup>

$\alpha$	$\lambda$	$\alpha$	$\lambda$
1.2311E+0	3.2881E+0	1.0075E-6	7.0465E-6
1.1486E+0	9.3805E-1	4.9894E-7	2.3190E-6
7.0701E-1	3.7073E-1	1.6352E-7	6.4480E-7
2.5209E-1	1.1118E-1	2.3355E-8	1.2649E-7
7.1870E-2	3.6143E-2	2.8094E-9	2.5548E-8
2.8291E-2	1.3272E-2	3.6236E-11	8.4782E-9
6.8382E-3	5.0133E-3	6.4577E-11	7.5130E-10
1.2322E-3	1.3655E-3	4.4963E-14	2.4188E-10
6.8409E-4	5.5158E-4	3.6654E-16	2.2739E-13
1.6975E-4	1.7873E-4	5.6293E-17	9.0536E-14
2.4182E-5	4.9032E-5	7.1602E-17	5.6098E-15
6.6356E-6	1.7058E-5		

$$f(t) = \sum_{i=1}^{23} \alpha_i e^{-\lambda_i t} \quad \text{MeV/Fission-s}$$

$$F(t, T) = \sum_{i=1}^{23} \frac{\alpha_i}{\lambda_i} e^{-\lambda_i t} (1 - e^{-\lambda_i T}) \quad \text{MeV/Fission}$$

$$F(t, \infty) \equiv F(t, 10^{13})$$

t and T in seconds

b

Read as  $1.2311 \times 10^0$

TABLE VIII

PARAMETERS FOR  $^{239}\text{Pu}$  THERMAL FISSION FUNCTIONS  $f(t)$  AND  $F(t, \infty)^a$

$\alpha$	$\lambda$	$\alpha$	$\lambda$
3.1094E-1	2.8480E+0	1.0141E-6	6.5786E-6
2.1395E-1	9.8330E-1	4.8987E-7	2.2253E-6
2.0240E-1	3.8966E-1	1.6170E-7	6.3618E-7
1.2174E-1	1.1978E-1	2.0947E-8	1.2722E-7
3.9701E-2	4.0829E-2	2.9902E-9	2.4609E-8
2.2748E-2	1.4287E-2	4.8496E-11	9.2396E-9
5.2320E-3	5.2952E-3	5.7292E-11	7.4498E-10
1.2591E-3	1.5235E-3	4.1331E-14	2.4251E-10
6.8417E-4	5.6352E-4	1.0908E-15	2.2044E-13
1.5842E-4	1.8578E-4	2.1519E-17	2.6819E-14
2.1323E-5	4.9377E-5	7.5638E-17	1.1834E-14
6.3717E-6	1.6710E-5		

a

$$f(t) = \sum_{i=1}^{23} \alpha_i e^{-\lambda_i t} \quad \text{MeV/Fission-s}$$

$$F(t, T) = \sum_{i=1}^{23} \frac{\alpha_i}{\lambda_i} e^{-\lambda_i t} (1 - e^{-\lambda_i T}) \quad \text{MeV/Fission}$$

$$F(t, \infty) \equiv F(t, 10^{13})$$

t and T in seconds

b

Read as  $3.1094 \times 10^{-1}$

These data are final with two minor qualifications: (1)  $^{235}\text{U}$  experiments at Berkeley are nearly complete and the results will generate a minor modification in the  $^{235}\text{U}$  data, expected to be well within the assigned uncertainties. (2) Experiments on  $^{239}\text{Pu}$  are in progress at IRT, ORNL, and LASL; these will ultimately modify the  $^{239}\text{Pu}$  values, if results are available before final acceptance of the recommended standard.

The  $^{238}\text{U}$  and  $^{239}\text{Pu}$  uncertainties are roughly a factor of two larger than those for  $^{235}\text{U}$  because only calculated values are used. For each nuclide, the values are 10.8  $\rightarrow$  8.9% between 1 and 10 s, 8.9  $\rightarrow$  6.4% between 10 and 100 s, and remain below 6% thereafter. These uncertainties are believed to be conservative.

#### REFERENCES

1. G. M. Hale, "R-Matrix Analysis of the  $^7\text{Li}$  System," to be published in Proc. International Specialists Symposium on Neutron Standards and Applications, Gaithersburg, MD (March 1977).
2. C. I. Baxman, G. M. Hale, and P. G. Young, Eds., "Applied Nuclear Data Research and Development, January 1-March 31, 1976," Los Alamos Scientific Laboratory report LA-6472-PR, p. 3 (1976).
3. J. Humblet and L. Rosenfeld, "Theory of Nuclear Reactions, I. Resonant States and Collision Matrix," Nucl. Phys. 26, 529 (1961).
4. G. M. Hale, "R-Matrix Methods for Light Systems," Nuclear Theory in Neutron Nuclear Data Evaluation, Vol. II, p. 1, IAEA, Vienna (1976).
5. D. I. Garber and R. R. Kinsey, "Neutron Cross Sections, Volume II, Curves," Brookhaven National Laboratory report BNL-325, 3rd Ed., p. 223 (1976).
6. R. C. Haight, S. M. Grimes, and J. D. Anderson, "Hydrogen and Helium Production Cross Sections for 15 MeV Neutrons on Stainless Steel 316 and 304," University of California Radiation Laboratory preprint 78783 (1976) and to be published in Nucl. Sci. & Eng.
7. F. D. Becchetti, Jr. and G. W. Greenlees, "Nucleon-Nuclear Optical-Model Parameters,  $A > 40$ ,  $E < 50$  MeV," Phys. Rev. 182, 1190 (1969).
8. D. Wilmore and P. E. Hodgson, "The Calculation of Neutron Cross Sections from Optical Potentials," Nucl. Phys. 55, 673 (1964).
9. F. G. Perey, "Optical-Model Analysis of Proton Elastic Scattering in the Range of 9 to 22 MeV," Phys. Rev. 131, 745 (1962).
10. C. Birattari, E. Gadioli, E. Gadioli Erba, A. M. Grassi Strini, G. Strini, and G. Tagliaferri, "Pre-Equilibrium Processes in (p,n) Reactions," Nucl. Phys. A201, 579 (1973).

11. G. B. Saha, N. T. Porile, and L. Yaffe, "(p,xn) and (p,pxn) Reactions of  $^{89}\text{Y}$  with 5-85 MeV Protons," Phys. Rev. 144, 962 (1966).
12. C. Birattari, E. Gadioli, A. M. Gtassi Stini, G. Tagliaferri, and L. Zetta, "(p,xn) Reactions Induced in  $^{169}\text{Tm}$ ,  $^{181}\text{Ta}$ , and  $^{209}\text{Bi}$  with 20 to 45 MeV Protons," Nucl. Phys. A106, 605 (1971).
13. E. D. Arthur and P. G. Young, "A New Statistical Preequilibrium Nuclear Model Code," Tran. Am. Nucl. Soc. 23, 500 (1976).
14. C. L. Dunford, "A Unified Model for Analysis of Compound Nucleus Reactions," Atomics International report AI-AEC-12931, July 15, 1970 (unpublished).
15. H. Rebel and G. W. Schweimer, "Improved Version of Tamura's Code for Coupled-Channel Calculations: JUPITOR Karlsruhe Version," Gesellschaft fur Kerforschung M.B.H. report KFK 133 (Feb. 1971).
16. D. M. Drake, G. F. Auchampaugh, E. D. Arthur, C. E. Ragan, and P. G. Young, "Double Differential Beryllium Neutron Cross Sections at Incident Neutron Energies of 5.9, 10.1, and 14.2 MeV," Los Alamos Scientific Laboratory report LA-6257 (1976).
17. R. A. Schrach, R. B. Schwartz, and H. T. Heaton, II, "Total Cross Sections of Silicon and Beryllium," Bull. Am. Phys. Soc. 16, 495 (1971).
18. G. F. Auchampaugh, S. Plattard, R. Extermann, and C. E. Ragan, III, "MeV Neutron Total Cross Sections of  $^9\text{Be}$ ,  $^{10,11}\text{B}$ , and  $^{12,13}\text{C}$ ," Proc. of the International Conference on the Interactions of Neutrons with Nuclei, Lowell, Mass., p. 1389 (1976).
19. S. G. Gardner, "Neutron Reactions on U-237," Lawrence Livermore Laboratory report UCID-16885 (August 1975) and "Recalculated Neutron Reaction Cross Section on U-239," Lawrence Livermore Laboratory report UCID-16920 (Sept. 1975).
20. J. Jary, "Statistical Model Evaluation of (n,xn) and (n,xnf) Cross Sections of the Uranium Isotopes U-232 to U-239 for 2 MeV to 15 MeV," Commissariat a L'Energie Atomique report CEA-R-4647 (1975).
21. F. Schmittroth and R. E. Schenter, "Application of Least-Squares Method to Decay Heat Evaluation," Hanford Engineering Development Laboratory report TC-796 (Feb. 1977).
22. G. I. Bell and S. Glasstone, Nuclear Reactor Theory (Van Nostrand Reinhold Company, New York 1970), p. 239 [especially Eq. (5.30)].
23. R. W. Hardie and W. W. Little, "1DX, A One-Dimensional Diffusion Code for Generating Effective Nuclear Cross Sections," Battelle Northwest Laboratory report BNWL-954 (March 1969).

24. R. B. Kidman and R. E. MacFarlane, "LIB-IV, A Library of Group Constants for Nuclear Reactor Calculations," Los Alamos Scientific Laboratory report LA-6260-MS (1976).
25. P. Walti and P. Kick, "MICROX, A Two-Region Flux Spectrum Code for the Efficient Calculation of Group Cross Sections," General Atomic report GA-A10827 (1972).
26. M. G. Stamatelatos, "Rational Approximations for Cross-Section Space-Shielding in Doubly Heterogeneous Systems," Nucl. Sci. Eng. 61, 543 (1976).
27. M. G. Stamatelatos and R. J. LaBauve, "Methods for Calculating Group Cross Sections for Doubly Heterogeneous Thermal Reactor Systems," Los Alamos Scientific Laboratory report LA-NUREG-6685-MS (1977).
28. D. W. Muir and P. G. Young, Eds. "Applied Nuclear Data Research and Development April 1 - June 30, 1975," Los Alamos Scientific Laboratory report LA-6123-PR (1975) Sec. VI.A, p. 12.
29. D. W. Muir and P. G. Young, Eds., "Applied Nuclear Data Research and Development April 1 - June 30, 1975," Los Alamos Scientific Laboratory report LA-6123-PR (1975) Sec. VI.B, p. 12.
30. D. R. Harris, W. A. Reupke, and W. B. Wilson, "Consistency Among Differential Nuclear Data and Integral Observations: The ALVIN Code for Data Adjustment, for Sensitivity Calculations, and for Identification of Inconsistent Data," Los Alamos Scientific Laboratory report LA-5987 (1975).
31. W. A. Reupke and D. W. Muir, "Consistency Analysis of Fusion Reactor Neutronics Data: Tritium Production," Trans. Am. Nucl. Soc. 23, 21 (1976).
32. D. W. Muir and M. E. Wyman, "Neutronic Analysis of a Tritium Production Integral Experiment," Proc. of Tech. of Controlled Thermonuclear Fusion Experiments and the Engineering Aspects of Fusion Reactors Conf., CONF-721111 (1972), p. 910.
33. M. E. Wyman, "An Integral Experiment to Measure the Tritium Production from <sup>7</sup>Li by 14-MeV Neutrons in a Lithium Deuteride Sphere," Los Alamos Scientific Laboratory report LA-2234-Rev (Nov. 1972).
34. W. A. Reupke and D. W. Muir, "Neutronic Data Consistency Analysis for Lithium Blanket and Shield Design," Proc. of the 2nd Topical Meeting on the Tech. of Controlled Nuclear Fusion, United States Energy Research and Development Administration report CONF-760935 (1977), Vol. 3, p. 861.
35. J. O. Hirschfelder, C. F. Curtiss, and R. B. Bird, Molecular Theory of Gases and Liquids (John Wiley and Sons, Inc., New York, 1954), Ch. 12.

36. P. A. Seeger and W. M. Howard, "Semiempirical Atomic Mass Formula," Nucl. Phys. A238, 491 (1975).
37. M. E. Meek and B. F. Rider, "Compilation of Fission Product Yields, Vallecitos Nuclear Center, 1974," General Electric Company report NEDO-12154-1, 74 NED6 (Jan. 1974).
38. A. Gilbert and A. G. W. Cameron, "A Composite Nuclear Level Density Formula with Shell Corrections," Can. J. Phys. 43, 1446 (1965).
39. J. Terrall, "Prompt Neutrons from Fission," Proc. of the International Atomic Energy Agency Symposium on Physics and Chemistry of Fission, Salzburg 1965, Vol. II, p. 3, IAEA Press, Vienna, Austria (1965).
40. D. G. Madland and I. Stewart, "Light Ternary Fission Products: Probabilities and Charge Distributions," Los Alamos Scientific Laboratory report LA-6783-MS (ENDF-247) (April 1977).
41. N. Tsoulfanidis, B. Wehring, and M. E. Wyman, "Measurement of Time-Dependent Energy Spectra of Beta Rays from Uranium-235 Fission Fragments," Nucl. Sci. Eng. 43, 4] (1971).
42. J. K. Dickens, T. A. Love, J. W. McConnell, R. M. Freestone, J. F. Emery, and R. W. Peele, "Fission Product Beta and Gamma Energy Release Quarterly Progress Report for July-September 1976," Oak Ridge National Laboratory report ORNL/NUREG/TM-65 (1976).
43. T. R. England and R. E. Schenter, "ENDF/B-IV Fission Product Files: Summary of Major Nuclide Data," Los Alamos Scientific Laboratory report LA-6116-MS (ENDF 223) (Oct. 1975).
44. T. R. England and M. G. Stamatelatos, "Multigroup Beta and Gamma Spectra of Individual ENDF/B-IV Fission-Product Nuclides," Los Alamos Scientific Laboratory report LA-NUREG-6622-MS (Dec. 1976).
45. R. J. LaBauve, T. R. England, M. G. Stamatelatos, and D. C. George, "Approximations to Summation Calculations of Delayed Energy and Spectra from Fission Products," Los Alamos Scientific Laboratory report LA-6684-MS (1977).
46. T. R. England, R. E. Schenter, and N. L. Whittemore, "Gamma and Beta Decay Power Following <sup>235</sup>U and <sup>239</sup>Pu Fission Bursts," Los Alamos Scientific Laboratory report LA-6021-MS (1976).
47. C. I. Baxman and P. G. Young, "Applied Nuclear Data Research and Development July 1 - September 30, 1976," Los Alamos Scientific Laboratory report LA-6723-PR (Feb. 1977), p. 21.